Spin-pair tunneling in Mn_3 single-molecule magnet

Yan-Rong Li, Rui-Yuan Liu, and Yun-Ping Wang
Beijing National Laboratory for Condensed Matter Physics, Institute of Physics, Chinese Academy of Sciences, Beijing 100190, People's Republic of China

(Received 31 October 2014; revised manuscript received 28 September 2015; published 20 October 2015)

We report spin-pair tunneling observed in a Mn_3 single-molecule magnet, which is a crystal with a two-dimensional network of identical exchange coupling. We observe a series of extra quantum tunnelings by the ac susceptibility measurements, and demonstrate that these are mainly thermally assisted tunnelings of a pair of two spins from the same initial state to the same final state simultaneously. The resonant field of spin-pair tunneling can be expressed as $H_z = lD/g\mu_0\mu_B + (n_\downarrow - n_\uparrow)JS/2g\mu_0\mu_B$, and the splitting interval ($|J|S/g\mu_0\mu_B$) is half that of the single-spin tunneling ($2|J|S/g\mu_0\mu_B$), which is analogous to the relationship between the magnetic flux quantum in superconductors ($h/2e$) and common metals (h/e).

DOI: 10.1103/PhysRevB.92.134415 PACS number(s): 75.45.+j, 75.50.Xx, 71.10.Li, 75.30.Et

As the counterpart of electron tunneling, spin tunneling in single-molecule magnets (SMMs) manifested by the quantum tunneling of magnetization (QTM) has recently attracted great interest [1–4]. In a system of individual SMMs, molecules are highly identical and magnetically independent of each other [2,3], hence the spin tunneling of the molecules doses not rely on its neighbors. Studies on dimer systems indicate that intermolecular exchange coupling has a great impact upon the observed QTM, where each part of the dimer acts as a field bias on its neighbors, shifting the tunneling resonances to new positions relative to the isolated molecules [5]. Previous studies also proposed spin-spin cross relaxation (SSCR) [6] and cotunneling [7], which provided complex pictures for the tunneling mechanism of two spins. For the SSCR [6], the tunnel transition reverses one of the two spins while the other spin changes to an excited state. For the cotunneling observed in $LiY_{0.998}Ho_{0.002}F_4$ [7], the distance and interaction between the two spins may change with different cotunneling. Recent research discovered that for SMMs with identical exchange coupling (IEC), the quantum tunneling of a single spin splits equally and depends heavily on its local spin environment (LSE) [8]. In this paper, we report spin-pair tunneling (SPT) in a Mn_3 SMM, with SPT denoted as the tunneling of a pair of spins from the same initial state to the same final state. The Mn_3 SMM is characteristic of a two-dimensional (2D) network with identical exchange coupling, hence one spin could pair with any of its neighboring spins to form an identical spin pair. Spin pairs in a Mn_3 SMM are analogous to Cooper pairs in superconductors, e.g., within a spin pair, the two spins tunnel together as a unit, which is observed as SPT. SPT is clearly identified in the ac susceptibility curves of a Mn_3 SMM, and evidenced by an abnormally high effective barrier at zero field as well.

A single crystal of a Mn_3 SMM has the formula $[Mn_3O(Et\text{-}sao)_3(MeOH)_3(ClO_4)]$. The preparation and crystal characteristics of a Mn_3 SMM have been reported earlier [8,9]. As described in Ref. [8], a Mn_3 SMM is a crystal with a 2D network of exchange coupling, in which each molecule is coupled with three neighboring molecules by hydrogen bonds in an *ab* plane, forming a honeycomblike structure viewed down along the *c* axis, therefore, the Mn_3 SMM is considered to be a crystal with IEC and is a model system of a simple Ising model. Each molecule has a ground spin state of $S = 6$ and a spin Hamiltonian of $\hat{\mathcal{H}} = -D\hat{S}_z{}^2 + g\mu_0\mu_B\hat{S}_zH_z$, where $D = 0.98$ K and $g = 2.06$ [8,10]. Due to the identical exchange coupling in a Mn_3 SMM, the quantum tunneling is equally split in the way of $(n_\downarrow - n_\uparrow)JS/g\mu_0\mu_B$, where $n_\downarrow$ and $n_\uparrow$ represent the numbers of spin-down and spin-up molecules neighboring to the tunneling molecule, and $J = -0.041$ K is the intermolecular exchange coupling constant [8].

Below the blocking temperature, SMMs show slow magnetic relaxation as spin flipping becomes difficult due to the high energy barrier, whereas SMMs show fast magnetic relaxation at a resonant tunneling field because of the quantum tunneling effect, which leads to steplike hysteresis loops [1–4]. Apart from dc susceptibility measurements, ac susceptibility measurements are also considered a good way to define the magnetic relaxation behavior in SMMs. Since the magnetic relaxation time obviously decreases at the resonant tunneling field, ac susceptibility demonstrates the peaks at resonant tunneling fields [11].

The blocking temperature of a Mn_3 SMM is estimated to be 3 K [8], hence we measured ac susceptibility at temperatures above 3 K. Figure 1(a) shows the field dependence of ac susceptibility at 7 K with a frequency of 9.99 kHz. The measurement was performed in a Quantum Design physical property measurement system (PPMS), employed with a 10 Oe amplitude excitation field, and the single crystal was oriented with the easy axis approximately parallel to the applied magnetic field. A series of peaks and dips have been observed in the χ' (real component) and χ'' (imaginary component) curves, respectively. The field dependence of χ''/χ' is shown in Fig. 1(b), which is considered a quantity proportional to the relaxation times [12], with χ''/χ' clearly demonstrating dips at the resonant fields. Apparently, in addition to the quantum tunnelings numbered 1, 3, 5, 7, 9, 11, and 15, which are due to the spin tunneling of a single Mn_3 molecule in different spin environments according to Ref. [8], four extra quantum tunnelings numbered 0, 2, 6, and 10, and located at 0, 0.34, 1.08, 1.80 T, respectively, are observed. Figures 2 and 3 present the field dependences of ac susceptibility measured (on another Mn_3 sample) at several temperatures and frequencies, which evidenced that the resonant fields are temperature and frequency independent. Figure 2 demonstrates the field dependence of ac susceptibility at different temperatures with

 ©2015 American Physical Society

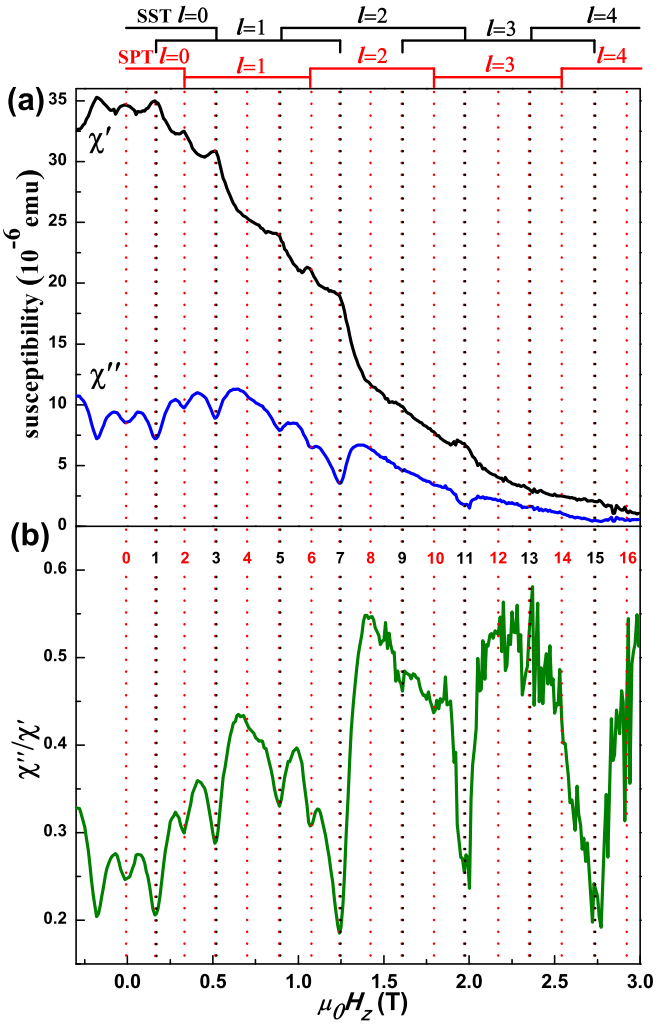

FIG. 1. (Color online) (a) Field dependence of ac susceptibility χ' (real component) and χ'' (imaginary component) from -0.3 to 3 T at 7 K, with a sweeping rate of 0.0005 T/s and frequency of 9.99 kHz. (b) Field dependence of χ'/χ'' from -0.3 to 3 T. The quantum tunnelings marked by the black and red dotted lines are single-spin tunneling (SST) and spin-pair tunneling (SPT) in different quantum tunneling sets, respectively [14]. Each observed tunneling is a combination of degenerate ground-state tunneling and a series of thermally assisted tunnelings.

a sweeping rate of 0.001 T/s and frequency of 9.99 kHz. It is seen that the quantum resonances appear within a temperature range of 4–8 K, and the positions of the quantum tunnelings are temperature independent. Figure 3 shows the field dependence of ac susceptibility at 7 K, with a sweeping rate of 0.001 T/s and different frequencies. It is seen that the positions of quantum tunnelings are frequency independent as well.

Distinctly, each of the extra quantum tunnelings mentioned above happens to appear at the midpoint between its two neighbor tunnelings. It is also noticeable that there is a quantum tunneling taking place at zero field. It had been suspected that a different type of isolated molecule might exist, which contributes to the extra tunnelings. However, this conjecture is dismissed, since the four-circle diffraction measurement shows that the sample is a good single crystal, and Fig. 1 shows

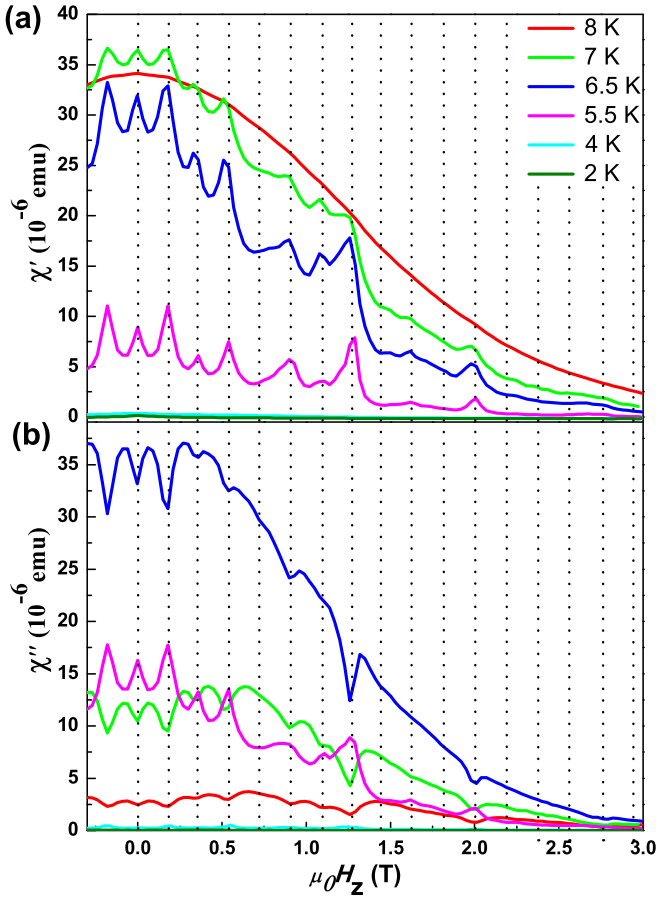

FIG. 2. (Color online) (a) Field dependence of ac susceptibility χ' (real component) from -0.3 to 3 T at different temperatures, with a sweeping rate of 0.001 T/s and frequency of 9.99 kHz. (b) Field dependence of ac susceptibility χ'' (imaginary component) from -0.3 to 3 T at different temperatures, with a sweeping rate of 0.001 T/s and frequency of 9.99 kHz.

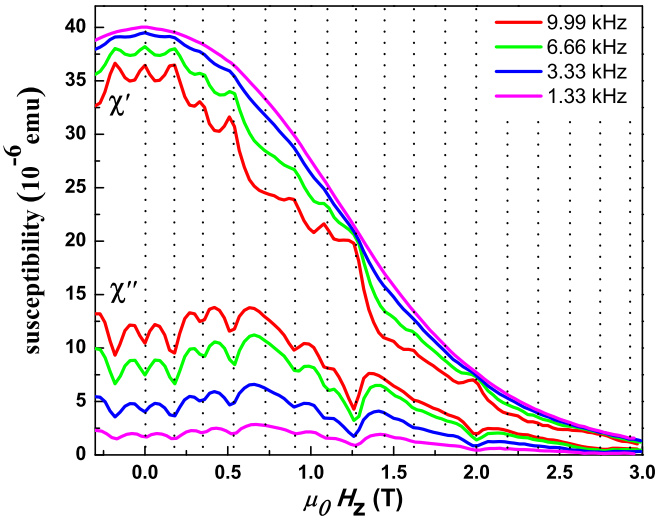

FIG. 3. (Color online) Field dependence of ac susceptibility χ' (real component) and χ'' (imaginary component) from -0.3 to 3 T at 7 K, with a sweeping rate of 0.001 T/s and different frequencies.

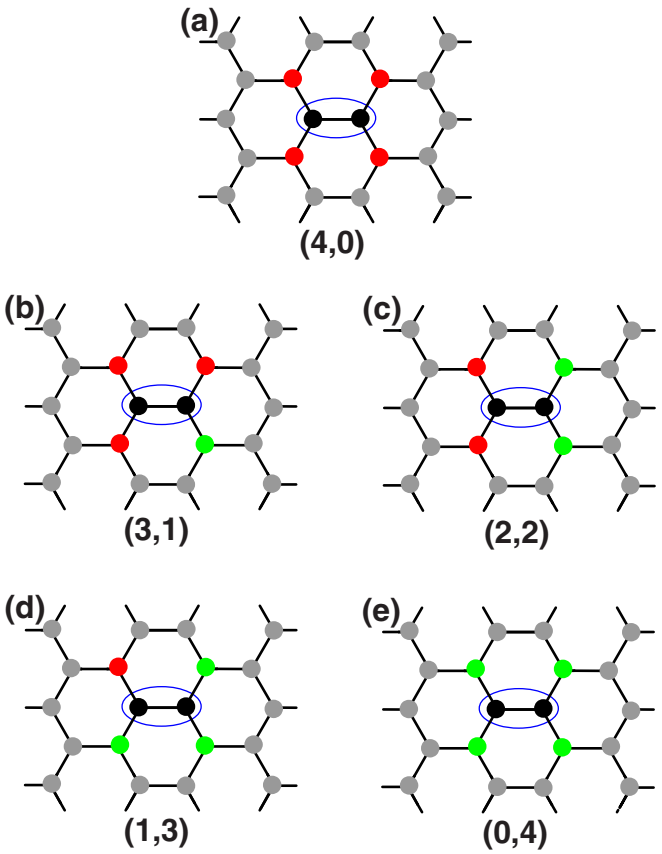

FIG. 4. (Color online) Sketch maps of five spin configurations with different LSEs $(n_\downarrow,n_\uparrow)$ for a pair of molecules; other equivalent spin configurations are not listed here for simplicity. The tunneling pair in the blue ellipse is marked in black, which could occupy either a spin-up or spin-down state simultaneously. Its four neighboring molecules, marked as red and green, occupy the spin-down and spin-up states, respectively. The direction of spin is perpendicular to the honeycomb lattice of the Mn_3 SMM. The black lines between the molecules represent the exchange couplings.

that every resonant field of the extra tunnelings is located at the midpoint between its two neighboring tunnelings. We will demonstrate in the following that these extra tunnelings as well as the tunneling occurring at zero field are spin-pair tunnelings (SPTs), i.e., cotunneling of two spins from the same initial state to the same final state simultaneously.

In a Mn_3 SMM, a single molecule has three exchange-coupled neighbors, hence, a pair of Mn_3 molecules has four exchange-coupled neighbors. Figure 4 demonstrates the five local spin environments (LSEs) of a spin pair marked in black, labeled as $(n_\downarrow,n_\uparrow)$, as described in Ref. [8].

For SMMs with IEC, the spin Hamiltonian of each molecule may be presented as

$$\hat{\mathcal{H}} = -D\hat{S}_z^2 + g\mu_0\mu_B\hat{S}_z H_z - \sum_{i=1}^{n} J\hat{S}_z\hat{S}_{iz} + \hat{\mathcal{H}}^{\text{trans}}, \qquad (1)$$

where n is the coordination number, $\hat{S}_z$ and $\hat{S}_{iz}$ are the easy-axis spin operators of the molecule and its ith exchange-coupled neighboring molecule, and $\hat{\mathcal{H}}^{\text{trans}}$ is the small off-diagonal perturbation term including high-order trigonal and hexagonal transverse operators [13], which allows the quantum tunneling to occur. For the single-spin tunneling (SST) from $|m\rangle$ to $|-m-l\rangle$ ($l = 0,1,2,3,\ldots$), where $m = -S, -(S-1)\ldots$ is the quantum number of the tunneling spins, the resonant field is determined by

$$H_z = lD/g\mu_0\mu_B + (n_\downarrow - n_\uparrow)JS/g\mu_0\mu_B, \qquad (2)$$

hence the quantum tunneling from the $|-6\rangle$ to $|6\rangle$ spin state is split into four, which occurs at $3JS/g\mu_0\mu_B$, $JS/g\mu_0\mu_B$, $-JS/g\mu_0\mu_B$, and $-3JS/g\mu_0\mu_B$, respectively [8]. However, for the SPT from $|m,m\rangle$ to $|-m-l,-m-l\rangle$, the resonant field is determined by

$$H_z = lD/g\mu_0\mu_B + (n_\downarrow - n_\uparrow)JS/2g\mu_0\mu_B, \qquad (3)$$

and hence the quantum tunneling from the $|-6,-6\rangle$ to $|6,6\rangle$ spin state is split into five, which occurs at $2JS/g\mu_0\mu_B$, $JS/g\mu_0\mu_B$, 0, $-JS/g\mu_0\mu_B$, and $-2JS/g\mu_0\mu_B$, respectively. Apparently, the splitting interval of SPT is $|J|S/g\mu_0\mu_B$, which is half that of SST.

Figure 1 demonstrates all SSTs and SPTs in different quantum tunneling sets [14], which are marked by black and red dotted lines, respectively. Within a SST set, the LSEs are (3,0), (2,1), (1,2), and (0,3) from the left to the right, respectively, and within a SPT set, the LSEs are (4,0), (3,1), (2,2), (1,3), and (0,4) from the left to the right, respectively. As a matter of fact, each tunneling demonstrated in Fig. 1 is a combination of degenerate ground-state tunneling and a series of thermally assisted tunnelings [1,15]. For example, SST $l = 0$ is a combination of all the degenerate tunnelings from $|m\rangle$ to $|-m\rangle$, and SPT $l = 0$ is a combination of all the degenerate tunnelings from $|m,m\rangle$ to $|-m,-m\rangle$. Since the axial anisotropy constant $D = 0.98$ K happens to be close to $4|J|S$ in a Mn_3 SMM [8,10], there are overlapped quantum tunnelings, for example, the quantum tunneling numbered 1 is a combination of the SST from the $|-6\rangle$ to the $|6\rangle$ spin state with LSE (1,2) and the SST from the $|-6\rangle$ to the $|5\rangle$ spin state with LSE (3,0) and the SPT from the $|-6,-6\rangle$ to the $|6,6\rangle$ spin state with LSE (1,3). With such a coincidence, the quantum tunnelings are taking place at fields with equal intervals, just as occurs in individual SMMs [1,4].

Of the overlapped tunnelings mentioned above, the contributions of the component quantum tunnelings are different due to the dependence of tunneling on the local spin environment and the potential barrier. It is noticed that the extra quantum tunnelings numbered with even numbers are purely SPT, while the quantum tunnelings numbered with odd numbers are a combination of SST and SPT. As reported in Ref. [8], the tunneling magnitude $\mathcal{T}$ of SST is described as

$$\mathcal{T} = \alpha N_{(n_\downarrow,n_\uparrow)} P_{|m_i\rangle\to|m_f\rangle}, \qquad (4)$$

where $N_{(n_\downarrow,n_\uparrow)}$ is the number of molecules with LSE $(n_\downarrow,n_\uparrow)$, and $P_{|m_i\rangle\to|m_f\rangle}$ is the tunneling probability of the molecule from the spin state $|m_i\rangle$ to $|m_f\rangle$, which is exponentially dependent on the effective barrier at the thermally activated tunneling region [11,16]. Note that Eq. (4) is applicable to SPT with the following transformation,

$$\mathcal{T} = \alpha N_{(n_\downarrow,n_\uparrow)} P_{|m_i,m_i\rangle\to|m_f,m_f\rangle}, \qquad (5)$$

where $N_{(n_\downarrow,n_\uparrow)}$ is the number of spin pairs with the LSE $(n_\downarrow,n_\uparrow)$, and $P_{|m_i,m_i\rangle\to|m_f,m_f\rangle}$ is determined by the aggre-

gated effective barrier of two SSTs, which can be deduced from $P_{|m_i,m_i\rangle\to|m_f,m_f\rangle} \propto P^2_{|m_i\rangle\to|m_f\rangle}$ and $P_{|m_i\rangle\to|m_f\rangle} \propto \exp(-U_{\rm eff}/k_BT)$. Apparently, the effective barrier of SPT is doubled, and hence is much higher than that of SST. According to Eqs. (4) and (5), the tunneling magnitudes of SST and SPT are heavily dependent on the numbers of single spins and spin pairs in the proper LSEs, respectively. At a high positive field, most molecules occupy the $|6\rangle$ spin state, therefore SSTs with LSE (0,3) are observable, such as the quantum tunnelings numbered 7, 11, and 15 observed in Fig. 1. On the other hand, only SPTs with LSE (0,4) are observed at high field, such as the quantum tunnelings numbered 6 and 10 in Fig. 1, and the expected quantum tunnelings numbered 4, 8, 12, 13, and 16 are not observed due to very small $N_{(n_\downarrow,n_\uparrow)}$, whereas the absence of SPT numbered 14 is due to a small signal-to-noise ratio.

As mentioned above, the effective barrier of SPT is doubled when compared to that of SST; this suggests that the tunneling probability of ground-state SPT is far less than that of SST, which is evidenced by the absence of SPT steps in hysteresis loops at low temperatures [8]. In the following, we demonstrate that the extra quantum tunnelings observed at 7 K are mainly thermally assisted SPT. Figure 5(a) shows the ac susceptibility of Mn_3 as a function of temperature with different frequencies at zero field, which demonstrates typical characteristics of SMMs: The dissipation peak in the χ''-T curve drops to a lower temperature at a higher frequency [16–19]. Figure 5(b) shows the fitting of the Arrhenius equation, which gives an effective barrier of $U_{\rm eff} = 55D$, in good agreement with the result mentioned in Ref. [9]. It is remarkable that $U_{\rm eff} = 55D$ is much larger than the anisotropy barrier $36D$, whereas $U_{\rm eff}$ is usually smaller than DS_z^2 in previous SMM studies [11,16]. As mentioned above, the effective barrier of SPT is supposed to be double that of SST, and since $U_{\rm eff} = 55D$ happens to be close to double the energy gap $(27D)$ between $|\pm6\rangle$ and $|\pm3\rangle$, it is evident that SPT leads to the observed tunneling at zero field, i.e., the spin relaxation at zero field should be dominated by two concerted spin flippings, and each flipping is of thermally assisted tunneling [11,16]. As shown in the inset of Fig. 5(b), the spin pair is initially thermally activated from the $|-6,-6\rangle$ state to the $|-3,-3\rangle$ state, next it tunnels to the $|3,3\rangle$ state, and it finally relaxes to the $|6,6\rangle$ state. This suggests that the spin relaxation of the Mn_3 SMM at high temperatures is dominated by thermally assisted tunneling instead of ground-state tunneling. Note that quantum tunneling takes place from the $|-3,-3\rangle$ to the $|3,3\rangle$ state in this relaxation process instead of other excited state tunnelings, which is consistent with the selection rule of C_3 symmetry in a Mn_3 SMM, i.e., those quantum tunnelings which satisfy $|\Delta m_s| = 3n$ are more enhanced due to the high-order trigonal and hexagonal transverse operators mentioned in Eq. (1) [13,20]. However, thermally assisted spin-pair tunneling is exponentially reduced when the temperature drops, and the probability of ground-state spin-pair tunneling is rather low due to the doubled barrier, leading to the absence of spin-pair tunneling at low temperatures [8,9].

SPT in a Mn_3 SMM is analogous to the tunneling of superconducting Cooper pairs, i.e., the Josephson effect in superconductors, in the sense of that the two spins of a spin pair entangle to behave as a unit, while the pairing could be formed between a spin and any of its neighboring spins, rather than a particular one. It is well known that both the net momentum and spin of the Cooper pairs are zero regardless of the value of the individual momentum and spin, which can be considered as a source of the momentum and spin entanglement state [21,22]. Similarly, the net exchange energy of the spin pair is a constant regardless of the individual exchange-energy distribution, for example, the SPT at zero field requires the LSE of spin pairs to be (2,2), which means the net exchange interaction between the spin pair and its neighbors is equal to zero, nevertheless, there are six equivalent neighboring spin distributions [Fig. 2(c) only shows one of them]. Furthermore, the splitting interval of SPT is $|J|S/g\mu_0\mu_B$, according to Eq. (3), which is half that of SST $(2|J|S/g\mu_0\mu_B)$, which is similar to the relationship between the magnetic flux quantum in superconductors $(h/2e)$ and common metals (h/e). The similarities and differences between SPT and the Josephson effect are shown in Table I. By giving a comparison of the spin-pair tunneling and tunneling of superconducting Cooper pairs, we hope to promote insight into the search for universal behaviors of pair tunneling in different systems and finding pair tunnelings in other systems.

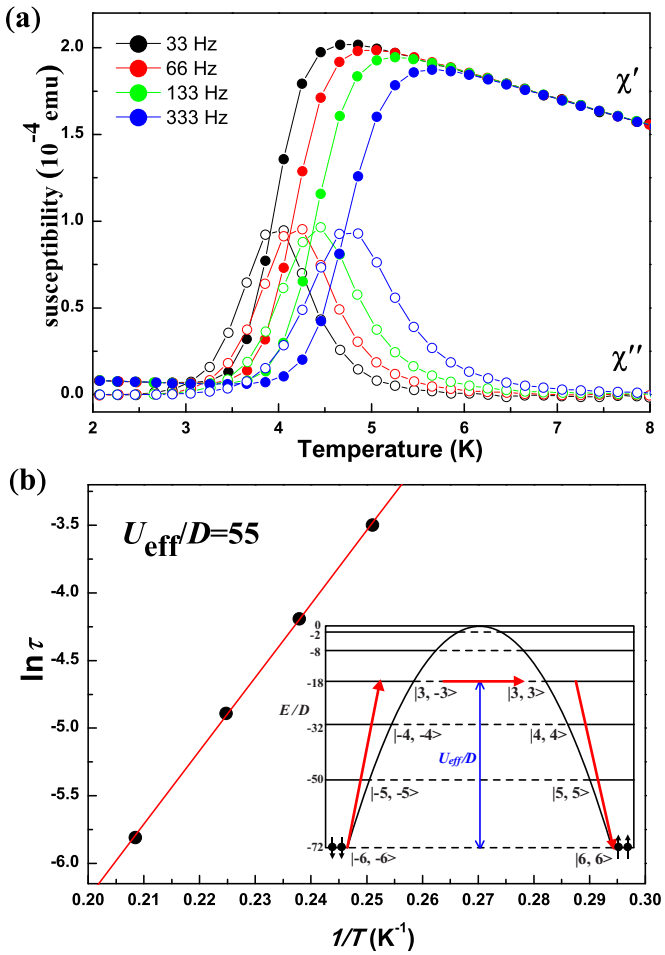

FIG. 5. (Color online) (a) Temperature dependence of ac susceptibility at different frequencies. (b) Plot of $\ln(\tau)$ vs $1/T$ with data obtained from ac susceptibility measurements, which gives $\tau_0 = 3.7 \times 10^{-8}$ s, $U_{\rm eff}/D = 55$, where $D = 0.98$ K. The inset shows the schematic drawing for the magnetic relaxation process within the temperature range 4–5 K.

TABLE I. The similarities and differences between spin-pair tunneling and the Josephson effect.

	Spin-pair tunneling	Josephson effect
Tunneling unit	Spin pair	Cooper pair
Pairing partner	Not fixed	Not fixed
Internal state of pair	Exchange-energy entanglement state	Momentum and spin entanglement state
Invariant of pair	Net exchange energy is a constant	Both net momentum and net spin are zero
Tunneling variable	Spin orientation of spin pair	Position of Cooper pair
Relationship with single particle	Splitting interval $\lvert J\rvert S/g\mu_0\mu_B$ is half that of single-spin tunneling ($2\lvert J\rvert S/g\mu_0\mu_B$)	Quantum flux $h/2e$ is half that in common metals (h/e)

These unique features of spin-pair tunneling are attributed to both the identical intermolecular exchange coupling and the identical spin states of the two spins in one spin pair, which should not be manifested in the spin-spin cross relaxation [6] and cotunneling processes [7] mentioned above. Since all the spin pairs in the SPT process are identical, the advantage of using SPT over cotunneling is similar to that of using SMMs over magnetic clusters for the study of quantum tunneling. Therefore, SPT is worth special attention and may open up new perspectives for quantum tunneling and inspire potential applications of molecular magnets.

This work was supported by the National Key Basic Research Program of China (No. 2011CB921702).

[1] J. R. Friedman, M. P. Sarachik, J. Tejada, and R. Ziolo, Phys. Rev. Lett. **76**, 3830 (1996).
[2] L. Thomas, F. Lionti, R. Ballou, D. Gatteschi, R. Sessoli, and B. Barbara, Nature (London) **383**, 145 (1996).
[3] C. Sangregorio, T. Ohm, C. Paulsen, R. Sessoli, and D. Gatteschi, Phys. Rev. Lett. **78**, 4645 (1997).
[4] K. L. Taft, C. D. Delfs, G. C. Papaefthymiou, S. Foner, D. Gatteschi, and S. J. Lippard, J. Am. Chem. Soc. **116**, 823 (1994).
[5] W. Wernsdorfer, N. Aliaga-Alcalde, D. N. Hendrickson, and G. Christou, Nature (London) **416**, 406 (2002).
[6] W. Wernsdorfer, S. Bhaduri, R. Tiron, D. N. Hendrickson, and G. Christou, Phys. Rev. Lett. **89**, 197201 (2002).
[7] R. Giraud, A. M. Tkachuk, and B. Barbara, Phys. Rev. Lett. **91**, 257204 (2003).
[8] Y. R. Li, R. Y. Liu, H. Q. Liu, and Y. P. Wang, Phys. Rev. B **89**, 184401 (2014).
[9] R. Inglis, L. F. Jones, G. Karotsis, A. Collins, S. Parsons, S. P. Perlepes, W. Wernsdorfer, and E. K. Brechin, Chem. Commun. **2008**, 5924 (2008).
[10] R. Inglis, S. M. Taylor, L. F. Jones, G. S. Papaefstathiou, S. P. Perlepes, S. Datta, S. Hill, W. Wernsdorfer, and E. K. Brechin, Dalton Trans. **2009**, 9157 (2009).
[11] F. Luis, J. Bartolome, J. F. Fernandez, J. Tejada, J. M. Hernandez, X. X. Zhang, and R. Ziolo, Phys. Rev. B **55**, 11448 (1997).
[12] T. Pohjola and H. Schoeller, Phys. Rev. B **62**, 15026 (2000).
[13] J. H. Atkinson, R. Inglis, E. del Barco, and E. K. Brechin, Phys. Rev. Lett. **113**, 087201 (2014).
[14] See Supplemental Material at http://link.aps.org/supplemental/10.1103/PhysRevB.92.134415 for a detailed description of the expected quantum tunnelings labeled from 0 to 16 in Fig. 1.
[15] S. Hill, S. Maccagnano, K. Park, R. M. Achey, J. M. North, and N. S. Dalal, Phys. Rev. B **65**, 224410 (2002).
[16] Y. R. Li, H. Q. Liu, Y. Liu, S. K. Su, and Y. P. Wang, Chin. Phys. Lett. **26**, 077504 (2009).
[17] A. M. Gomes, M. A. Novak, R. Sessoli, A. Caneschi, and D. Gatteschi, Phys. Rev. B **57**, 5021 (1998).
[18] X. X. Zhang, J. M. Hernandez, E. del Barco, J. Tejada, A. Roig, E. Molins, and K. Wieghardt, J. Appl. Phys. **85**, 5633 (1999).
[19] S. Accorsi *et al.*, J. Am. Chem. Soc. **128**, 4742 (2006).
[20] J. J. Henderson, C. Koo, P. L. Feng, E. del Barco, S. Hill, I. S. Tupitsyn, P. C. E. Stamp, and D. N. Hendrickson, Phys. Rev. Lett. **103**, 017202 (2009).
[21] J. Bardeen, L. N. Cooper, and J. R. Schrieffer, Phys. Rev. **108**, 1175 (1957).
[22] A. Hayat, H- Y. Kee, K. S. Burch, and A. M. Steinberg, Phys. Rev. B **89**, 094508 (2014).